Journal of Materials Chemistry C

PAPER

View Article Online
View Journal | View Issue

Cite this: J. Mater. Chem. C, 2017, 5, 2807

Morphological regulation improved electrical conductivity and electromagnetic interference shielding in poly(L-lactide)/poly(ε-caprolactone)/carbon nanotube nanocomposites *via* constructing stereocomplex crystallites†

Kai Zhang,[a] Hai-Ou Yu,[a] Yu-Dong Shi,[a] Yi-Fu Chen,[a] Jian-Bing Zeng,[a] Jiang Guo,[b] Bin Wang,[bc] Zhanhu Guo*[b] and Ming Wang*[a]

Received 23rd January 2017,
Accepted 17th February 2017

DOI: 10.1039/c7tc00389g

rsc.li/materials-c

Morphological control of conductive networks in conductive polymer composites has been demonstrated to efficiently improve their electrical performance. Here, morphological regulation used for the formation of conductive networks occurs in poly(L-lactide)/poly(ε-caprolactone) (PLLA/PCL) blends when stereocomplex crystallites (SCs) are formed in the PLLA phase. The SCs formed during the melt-processing increase the viscosity and elasticity of the PLLA phase, which makes the PLLA domains shrink and the PCL phase becomes continuous from the previously dispersed phase. As a result, for PLLA/PCL/multi-walled carbon nanotube (MWCNT) nanocomposites, the MWCNTs prefer to disperse in the PCL phase *via* morphological regulation. The electrical conductivity and the electromagnetic interference (EMI) shielding effectiveness (SE) of the PLLA/PCL/MWCNT nanocomposites can be abruptly increased and attributed to the simultaneous organization of conductive paths when the continuous PCL phase develops. For example, the electrical conductivity and the EMI SE of the PLLA/PCL/MWCNT nanocomposites increased from 2.1×10^{-12} S m^{-1} and 5.3–8.6 dB to 0.012 S m^{-1} and ~17 dB, respectively, with 0.8 wt% MWCNTs when adding 20 wt% poly(D-lactide) (PDLA) to the PLLA phase. Furthermore, the percolation threshold of the nanocomposites was reduced from 0.13 to 0.017 vol% by adding 20 wt% poly(D-lactide) (PDLA) to the PLLA phase.

1. Introduction

Conductive polymer composites (CPCs) with high electrical conductivity have potential in a wide range of applications such as antistatic materials,[1–3] electromagnetic interference (EMI) shielding,[4–6] sensors[7–11] and conductors.[12–14] Conductive fillers are normally randomly dispersed in the insulating polymer matrix and generally require high loadings to attain an insulator/conductor transition. A high content of conductive fillers will always lead to high melt viscosities, low economic affordability and inferior mechanical properties. The morphological control of conductive networks in CPCs has been well demonstrated to efficiently improve the electrical performance and sufficiently solve these problems.[15–21] Recently, blending of two or more polymer components has become a novel method to morphologically control the design and fabrication of conductive networks selectively dispersed at one of the polymer phases or at the interfaces, such as double percolation structures[22–27] and segregated structures.[28–33]

The double percolation structures are formed in a co-continuous immiscible polymer blend with conductive fillers selectively located in one continuous phase. The percolation of the whole sample and the percolation of conductive particles in the selected phase are simultaneously achieved in these blends.[22] The location of conductive fillers depends on the polymer–filler interactions that reduce the interfacial energies.[23] The final structures have remarkably increased conductivity and a significantly decreased percolation threshold.[26] The electrical conductivity can be further enhanced if the conductive fillers are only selectively distributed at the continuous interface of the co-continuous polymer blend.[27] In segregated structures,

[a] Key Laboratory of Applied Chemistry of Chongqing Municipality, School of Chemistry and Chemical Engineering, Southwest University, Chongqing, 400715, China. E-mail: mwang@swu.edu.cn
[b] Integrated Composites Laboratory (ICL), Department of Chemical and Biomolecular Engineering, University of Tennessee, Knoxville, TN, 37996, USA. E-mail: nanomaterials2000@gmail.com, zguo10@utk.edu
[c] Engineered Multifunctional Composites (EMC) Nanotechnology LLC, Knoxville, TN 37934, USA

† Electronic supplementary information (ESI) available. See DOI: 10.1039/c7tc00389g

the conductive fillers are primarily located at the interfaces among the polymeric matrix particles. The conductive fillers with confined dispersion in the interfacial regions construct dense conductive networks.[28] Finally, the CPCs with segregated electrically conductive network structures have high electrical conductivity and low percolation concentration at low filler loadings.[29] Thus, the electrical conductivity of CPCs can be enhanced by adding a very small amount of fillers and by controlling their distribution and forming conductive networks (double percolation structures, segregated structures, *etc.*) in a polymer matrix.

Recently, electromagnetic pollution has become a serious threat to health. CPCs have been thought to be powerful candidates to solve this pollution problem.[34] However, to achieve an adequate electromagnetic interference (EMI) shielding effectiveness (SE), conventional CPCs are usually filled with highly conductive fillers, which will sacrifice the economic feasibility and mechanical performance.[35–37] To date, a high EMI SE at a low filler loading for CPCs remains a challenge. CPCs with segregated conductive networks or double percolation structures show potential to solve this problem, because of their numerous interactive interfaces.[38–40] Electromagnetic microwaves can be efficiently attenuated by reflecting, scattering and absorbing many times at interfaces and conductive filler surfaces.[41]

Biocompatible and biodegradable blends of poly(L-lactide) (PLLA) and poly(ε-caprolactone) (PCL) have generated a great deal of interest since their blends have demonstrated their easy morphological control for property modification. The final morphology of the PLLA/PCL blends mainly depends on the content of PCL and the crystalline behavior of PLLA.[42–44] Recently, carbon nanotube (CNT) filled PLLA/PCL systems have become very popular to obtain materials with high electrical conductivity because the CNTs are favorably localized in the PCL phase and form double percolation structures, and the final composites are biodegradable as well.[45,46] The electrical performance can be further enhanced by controlling the number of CNTs at the interface of the co-continuous PLLA/PCL blends through the migration process of CNTs from the unfavorable PLLA phase to the favorable PCL phase.[47] Furthermore, the electrical conductivity of the PLLA/PCL/CNTs nanocomposites can be well tuned by controlling their morphologies *via* the choice of ratio of PLLA to PCL.[48]

Interestingly, stereocomplex crystallites (SCs) can be easily formed when poly(D-lactide) (PDLA) chains are introduced into the PLLA chains during melt processing because their much higher melting temperature (T_m) relative to homocrystallites (HCs) makes them able to survive in the melts of asymmetric PLLA/PDLA blends.[49–51] The formation of SCs dramatically increases the viscosity of the PLLA matrix and subsequently induces the morphological change in the PLLA-based blends.[52] Inspiringly, the SCs can act as efficient rheological modifiers[53] and enable morphology regulation in the PLLA-based blends by only constructing enough SCs in the PLLA phase without changing their mixing ratio. The formed SCs in the PLLA phase will probably increase the elasticity of the PLLA phase and serve as nucleating sites to increase the crystallinity of HCs with a processing temperature between the T_m of HCs and SCs. Thus, it is possible to realize morphological regulation in the PLLA/PCL blends by the SCs from a PLLA-rich morphology to a PCL-rich morphology. Furthermore, the CNTs show high interfacial interaction with the PCL chains and prefer to disperse in the PCL phase.[47] Thus, the morphological regulation will probably benefit the formation of double percolation structures and/or segregated structures in the PLLA/PCL/CNT nanocomposites and finally increase their electrical conductivity. However, this has not been reported yet.

Herein, morphological regulation was achieved with the dispersed phase of PCL becoming a continuous phase. The phase transition was realized by increasing both the viscosity and the elasticity of the PLLA phase in the PLLA/PCL blends *via* constructing SCs in the PLLA phase. The dispersion of multi-walled carbon nanotubes (MWCNTs) in the PCL phase was studied. The nature of the abruptly improved electrical conductivity of the PLLA/PCL/MWCNT nanocomposites without changing the mixing ratio was disclosed. The effect of the amount of PDLA on the morphology and the phase was investigated. Meanwhile, the electrical conductivity and EMI shielding behaviors of these unique nanocomposites were also reported.

2. Experimental

2.1 Materials

Poly(L-lactide) (PLLA, trade name 4032D) with 98.7 mol% L-isomeric content, a weight-average molecular weight (M_w) of 2.10×10^5 g mol^{-1} and a density of 1.24 g cm^{-3} was purchased from Nature Works LLC (USA). PDLA with a M_w of 1.34×10^5 g mol^{-1} was obtained from Jinan Dai Gang Biological Engineering Co. Ltd (China). Poly(ε-caprolactone) (PCL, trade mark Esun500C) with a molecular weight of 5.0×10^4 g mol^{-1} and a density of 1.15 g cm^{-3} was purchased from Guanghua Weiye industrial Co., Ltd (Shenzhen, China). MWCNTs (NC 7000) with an average diameter of 9.5 nm, an average length of 1.5 μm, a surface area of 250–300 m^2 g^{-1}, and a carbon purity of 90% were supplied by Nanocyl SA (Belgium). The density of the MWCNTs used in this work was about 1.75 g cm^{-3}.[54,55]

2.2 Sample preparation

The PCL, PLLA and PDLA were dried at 40, 80 and 80 °C for 12 h in a vacuum oven before use, respectively. The blends of PLLA and PCL with 70/30, 60/40 and 50/50 weight ratios without MWCNTs were melt mixed in a chamber (HAPRO-200A) with a mixing rotation of 80 rpm for 9 min at 180 °C to study the effect of components on the morphology of the PLLA/PCL blends. For the samples without PDLA, PLLA (60 wt%) was first added to the mixing chamber with a mixing rotation of 80 rpm for 3 min at 180 °C. After that, the PCL (40 wt%) and MWCNTs were added simultaneously at the same mixing rotation and temperature for 6 min. For convenience, the obtained PLLA/PCL/MWCNT nanocomposites were marked as PLLA/PCL/*z*MWCNTs, where *z* represents the content of MWCNTs.

For the samples with PDLA, the PLLA and PDLA (the total percent of PLLA and PDLA was 60 wt%) were first mixed at the

same rotation speed and temperature for 3 min, and then mixed with PCL (40 wt%) and MWCNTs for 6 min. For convenience, the obtained (PLLA + PDLA)/PCL/MWCNT nanocomposites were marked as (*x*PLLA + *y*PDLA)/PCL/*z*MWCNTs, where *x* and *y* represent the content of PLLA and PDLA, respectively. In order to study the effect of PDLA on the morphological (including phase) transformation, the *x*/*y* values were selected to be 45/15, 48/12, 51/9, 54/6 and 57/3. All the mixtures were dried at 40 °C for 6 h in a vacuum oven and then compression molded into a ∅65 mm circular sheet with a thickness of 1.5 mm on a hot-press at 180 °C and 10 MPa and finally cooled down on a cold-press at room temperature (20 °C) and 10 MPa for 4 min at a cooling rate of ~40 °C min^{-1}. These compression-molded samples were used for the conductive, morphological and rheological evaluation. As the compression temperature (180 °C) was between the melting point (T_m) of HCs (165 °C) and SCs (222 °C), the surviving SCs could act as physical cross-linking points to increase the viscosity and elasticity of the PLLA phase and cause morphological regulation to occur during the processing.

2.3 Characterization

To study the formation of SCs in the (*x*PLLA + *y*PDLA)/PCL/0.08MWCNT nanocomposites, WAXD patterns of the samples were characterized using an X-ray diffractometer (Shimadzu XRD-7000), using Cu Kα radiation with a wavelength of 1.54 Å. The testing was performed over the angle range 2θ = 5–40° at 40 kV and 40 mA.

The nonisothermal crystallization behaviors of the samples were performed using a NETZSCH DSC-214 differential scanning calorimeter in a dry nitrogen atmosphere. For each measurement, about 5 mg in an aluminum pan was first heated from 25 to 190 °C at a heating rate of 10 °C min^{-1} and held for 3 min to remove thermal history, then cooled down to 25 °C at a cooling rate of 10 °C min^{-1}, and finally reheated to 250 °C at a heating rate of 10 °C min^{-1}. For the samples without PDLA, the degree of crystallinity (X_c) was evaluated according to eqn (1) from the second heating curve.[52]

$$X_c = \frac{\Delta H_m - \Delta H_c}{w_f \Delta H_m^\circ} \quad (1)$$

where ΔH_m, ΔH_c, w_f and ΔH_m° are the measured enthalpies of melting, the measured enthalpies of cold crystallization, the weight percent of the PLLA matrix, and the melting enthalpy of 100% crystalline PLLA of 93.7 J g^{-1},[56] respectively. For the samples with PDLA, the degrees of crystallinity for HCs and SCs were estimated by comparing melting enthalpies to the corresponding value of an infinitely large crystal, taken as 93.7 and 142 J g^{-1} for HCs and SCs, respectively.[57]

The electrical conductivities of the samples were measured by a digital high resistance machine (PC68, Shanghai Precision Instrument Manufacture, China) at room temperature (23 °C). At least five specimens were tested and average data were reported.

The morphologies and distribution of MWCNTs of the samples were observed by a field-emission scanning electron microscope (SEM, JEOL, JSM-7800F) with an accelerating voltage of 5 or 10 kV. The specimens were firstly cryo-fractured in liquid nitrogen, and then coated with a layer of gold in a vacuum chamber before the SEM observation.

The electromagnetic interference (EMI) shielding effectiveness (SE) of the composites was evaluated using an Agilent N5230A vector network analyzer with transmission-reflection mode[58–60] at room temperature in the frequency range of 8–12 GHz. The samples of 13 mm diameter and 1.5 mm thickness were directly cut from the ∅65 mm circular sheets maintained in the preparation section for the EMI test. The total EMI SE was also calculated, and it was defined as the logarithmic ratio of incoming (P_{in}) to outgoing power (P_{out}) of electromagnetic radiation.[61]

$$SE_{total} = 10 \log(P_{in}/P_{out}) = SE_A + SE_R + SE_M \quad (2)$$

where SE_A, SE_R, and SE_M are the absorption shielding, reflection shielding, and multiple reflections shielding, respectively. SE_M usually can be neglected when $SE_{total} > 10$ dB. The SE_A and SE_R can be obtained using eqn (3) and (4), respectively.

$$SE_A = -10 \log(T/(1 - R)) \quad (3)$$

$$SE_R = -10 \log(1 - R) \quad (4)$$

where *T* and *R* are the power coefficients of transmissivity and reflectivity, respectively, which are calculated by the measured scattering parameters (S_{11} and S_{21}).

3. Results and discussion

3.1 Morphological transformation induced by polymorphic crystalline structures

The (*x*PLLA + *y*PDLA)/PCL/0.08MWCNT nanocomposites with various amounts of PDLA were prepared by melt-blending and compression molded at 180 °C and then cooled down at a rate of ~40 °C min^{-1}. The SCs can be easily formed through cocrystallization under these melt-processing conditions.[52] The WAXD results provide clear-cut evidence for the formation of

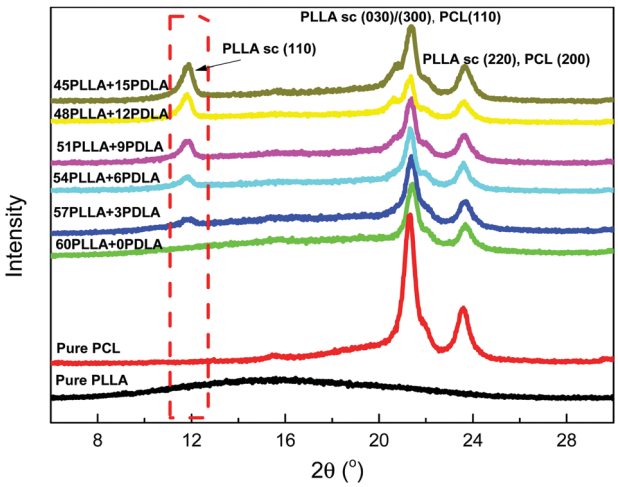

Fig. 1 WAXD profiles of the (*x*PLLA + *y*PDLA)/PCL/0.08MWCNT nanocomposites with various ratios of PLLA to PDLA after compression molding.

SCs in the nanocomposites, Fig. 1. There are no characteristic crystalline peaks found in pure PLLA, indicating that the HCs of pure PLLA are hardly formed under this rapid cooling rate. The characteristic peaks in the patterns of pure PCL at 21.4° and 23.7° are assigned to the (110) and (200) planes of crystallites.[62] The characteristic peaks are found in the patterns of the (*x*PLLA + *y*PDLA)/PCL/0.08MWCNT nanocomposites with PDLA at about 11.9°, 21.4° and 23.7°, corresponding to the (110), (300)/(030), and (220) planes of SCs.[63,64] The results indicate that the characteristic diffractions of (110) and (200) planes in the PCL crystallites are overlapped by the characteristic diffractions of the (300)/(030), and (220) planes in SCs. However, the characteristic diffractions of the (110) plane in SCs are very clear to find in the samples with PDLA and become stronger upon increasing the ratio of PDLA to PLLA from 5/95 to 25/75. The results indicate that SCs can be successfully formed in the (*x*PLLA + *y*PDLA)/PCL/0.08MWCNT nanocomposites at a cooling rate of ~40 °C min^{-1} and the number of SCs increased upon increasing the amount of PDLA.

The melting behavior of the nanocomposites with or without PDLA was also investigated with different contents of MWCNTs. For the samples without PDLA, the melting behaviors of the PCL phase and the PLLA phase are independent of the content of MWCNTs, Fig. 2a. The melting temperature of the PCL phase in all the PLLA/PCL/*z*MWCNT nanocomposites is ~57 °C. The crystallinities of the PCL phases are also close to each other. The cold crystallization of the PLLA phase happens in all the samples. The melting point of PLLA crystallites in all samples is ~169 °C, indicating the formation of HCs after the cold crystallization. The calculated crystallinity of the samples marked in the melting curves is very low (<2.0%), showing that few PLLA chains were crystallized at the cooling rate of 10 °C min^{-1}.

For the samples with PDLA, although the MWCNTs exhibit little effect on the melting behavior of the (48PLLA + 12PDLA)/PCL/*z*MWCNT nanocomposites, the melting behavior of the PLLA phase is different to that for the samples without PDLA, Fig. 2b. The samples were first heated to 190 °C which was higher than the melting temperature of HCs and lower than that of SCs. Thus, the SCs survived at this temperature. The samples were subsequently cooled down to 25 °C. The surviving SCs show efficient nucleating effects on HCs. The crystallization temperature of 119 °C was found in the samples with PDLA but absent in the samples without PDLA (Fig. S1, ESI†). Finally, the samples were melted again to 250 °C. The melting points of HCs and SCs, which are both found in the samples with PDLA, are 165 and 222 °C, respectively. The crystallinity of HCs is about 19% while the crystallinity of SCs is nearly 21% for all the samples. The results indicate that SCs were indeed formed in the samples with PDLA during the sample preparation and the SCs also showed an efficient nucleating effect on the crystallization of HCs.

The formed SCs in the samples with PDLA increase the viscosity and elasticity of the PLLA phase (Fig. S2, ESI†), which will cause a morphological transformation to occur in the PLLA/PCL blends by inducing SCs in the PLLA phase, according to the classical Paul–Barlow theory.[65] Fig. 3 shows the morphological

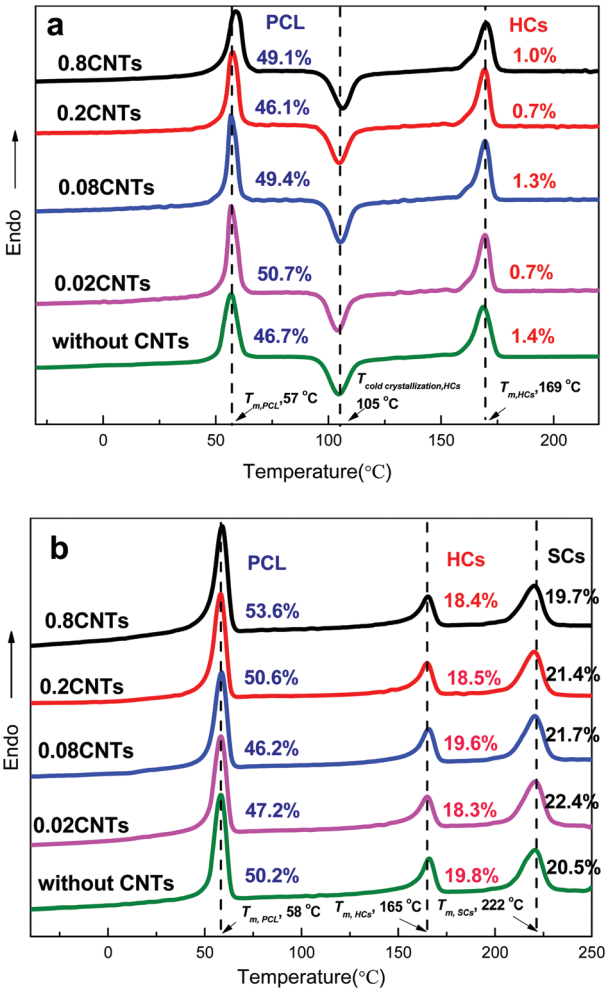

Fig. 2 DSC melting curves of the (a) PLLA/PCL/*z*MWCNT nanocomposites and (b) (48PLLA + 12PDLA)/PCL/*z*MWCNT nanocomposites collected upon second heating at a heating rate of 10 °C min^{-1}. The HCs and SCs in the figures represent the homocrystallites and stereocomplex crystallites of PLLA, respectively.

change with different ratios of the two polymers and the morphological transformation induced by the formation of SCs. PCL droplets dispersed in the PLLA matrix are observed for the PLLA/PCL 70/30 and 60/40 blends (Fig. 3a and b). The elongational co-continuous morphology is found in the PLLA/PCL 50/50 blends (Fig. 3c and d). The results indicate that morphological transformation can occur in the PLA/PCL blends *via* changing the components. However, the results are different from the reported work showing the elongational co-continuous morphologies found in the PLLA/PCL 60/40 blends and also 50/50 blends.[48] The ratio difference of PLLA/PCL for the morphological transformation is mainly related to the viscosity ratio difference (the viscosity ratio of PLA and PCL components is about 23 in the literature; however, the viscosity ratio is about 5.7 in our work) and the PLLA elasticity formed at different shear rates. Thus, the PLLA/PCL 60/40 blends with sea-island morphology were selected in this study to investigate the morphology transformation by inducing SCs in the PLLA phase and further to improve the electrical conductivity of the PLLA/PCL/MWCNT nanocomposites.

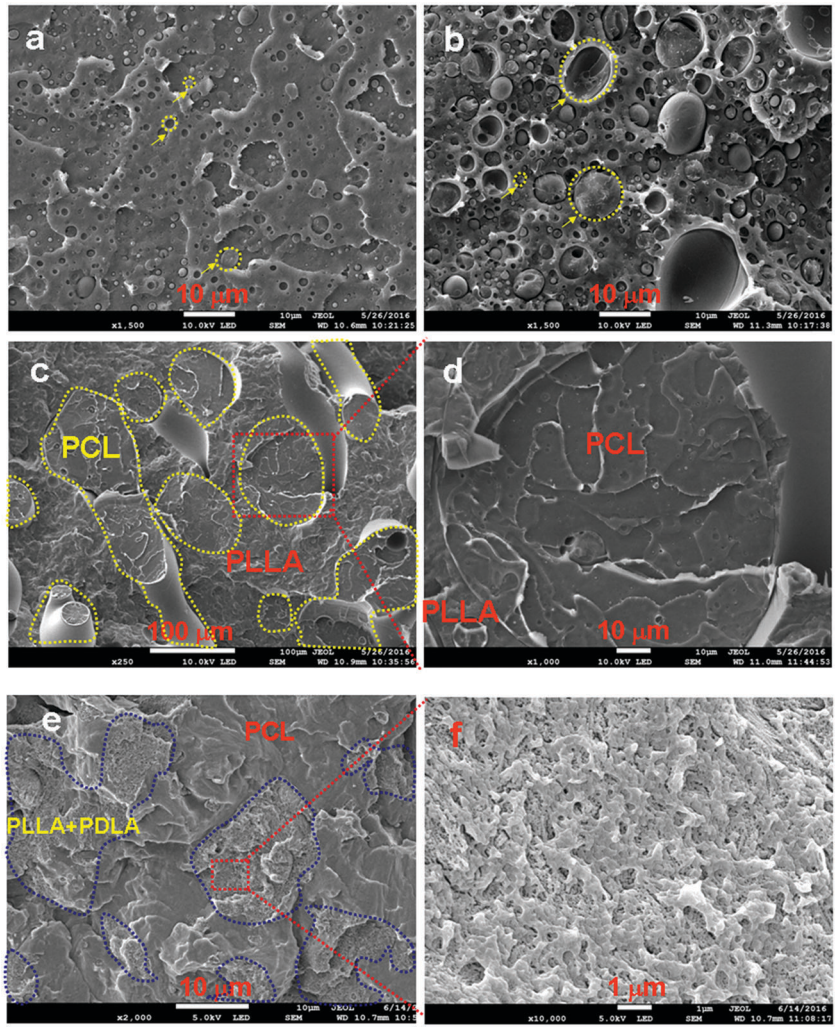

Fig. 3 Morphology of PLLA/PCL blends with a mixing ratio of PLLA to PCL: (a) 70/30, (b) 60/40, (c) 50/50; and (d) the magnification of the PCL phase in (c). Morphology of the (48PLLA + 12PDLA)/PCL blends (e) and the magnification of the (PLLA + PDLA) phase (f). The yellow curves encircle the PCL phase, while the blue curves encircle the (PLLA + PDLA) phase.

The incorporation of PDLA in PLLA to form SCs will enhance the elasticity and viscosity of the PLLA melt which will cause morphological transformation in the PLLA/PCL 60/40 blends. Fig. 3e and f show the dispersion PLLA + PDLA phase (PLLA/PDLA 48/12) and the continuous PCL phase. The PLLA + PDLA domains show relatively rough surfaces after cryo-fracturing because of the crosslinking effect of SCs. Furthermore, the MWCNTs prefer to disperse in the PCL phase, which is supported by the thermodynamic and kinetic analysis (ESI†). Thus, the morphological transformation to form the continuous PCL phase and the restriction of MWCNTs in the PCL phase are helpful to form efficiently the conductive networks in the PLLA/PCL/MWCNT nanocomposites by inducing the SCs in the PLLA phase.

3.2 Effect of PDLA content on the morphological transformation

In order to investigate the effect of PDLA content on the morphological transformation, (PLLA + PDLA)/PCL 60/40 blends with different percentages of PDLA were prepared under the same conditions. Fig. 4 shows the SEM images of the samples without PDLA and with 5, 10, 15, 20 and 25 wt% PDLA in the PLLA phase. Small PCL droplets are found to be randomly dispersed in the PLLA continuous phase for the samples without PDLA and with 5 wt% PDLA (Fig. 4a and b). Upon increasing the amount of PDLA, the small PCL droplets aggregate together to form large strips in the samples with 10 and 15 wt% PDLA (Fig. 4c, c′, d and d′). The co-continuous morphology is found in the samples with 20 wt% PDLA (Fig. 4e and e′). The PLLA phase becomes individual droplets dispersed in the PCL continuous phase when the amount of PDLA reaches 25 wt% (Fig. 4f and f′). The results indicate that the size of the PCL phase increases upon increasing the amount of PDLA and finally forms a continuous PCL phase when enough PDLA is added. This morphological transformation is mainly related to the increased viscosity and elasticity of the PLLA phase induced by the formation of SCs. The viscosity and elasticity of the PLLA phase nearly linearly increase upon increasing the amount of PDLA. As a result, the morphology of the PLLA-based polymer blends can be regulated by adding

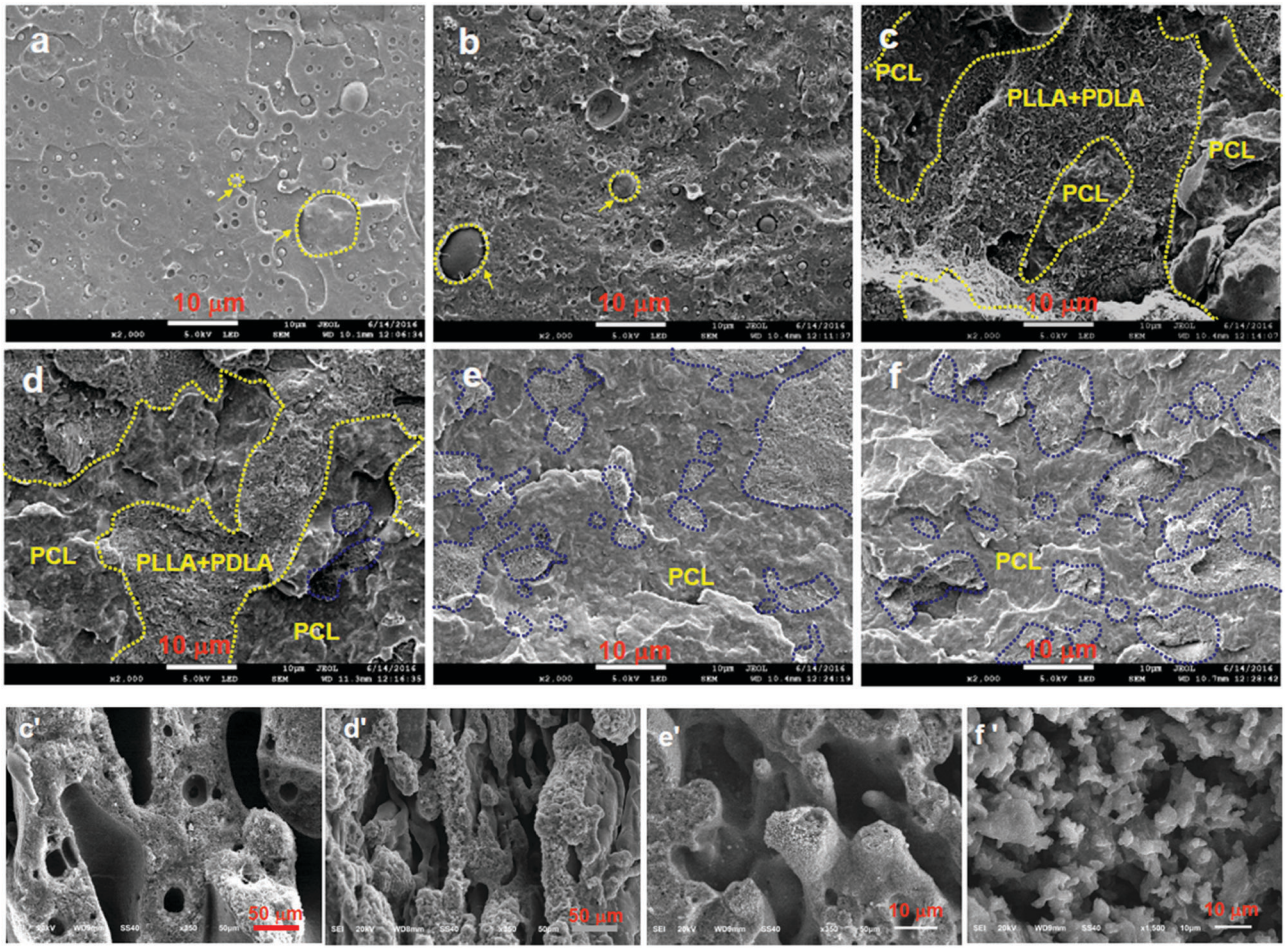

Fig. 4 Effect of PDLA loading on the morphology of (PLLA + PDLA)/PCL 60/40 blends: (a) without, and with (b) 5 wt%, (c) 10 wt%, (d) 15 wt%, (e) 20 wt% and (f) 25 wt% PDLA in the PLLA phase. The etched surface (the PCL phase is removed) of the composites with (c′) 10 wt%, (d′) 15 wt%, (e′) 20 wt% and (f′) 25 wt% PDLA in the PLLA phase. The yellow curves encircle the PCL phase, while the blue curves encircle the PLLA phase.

different amounts of PDLA, which can be used to modify the properties of the PLLA-based polymer blends.

Remarkably, the morphological transformation to form the PCL continuous phase is prone to organize double percolation structures and/or segregated structures in the PLLA/PCL/MWCNT nanocomposites and finally obtain highly conductive materials. Fig. 5 shows the effect of PDLA content on the electrical conductivity of the (*x*PLLA + *y*PDLA)/PCL/MWCNT nanocomposites with the same MWCNT content of 0.08 wt%. The electrical conductivity of the nanocomposites first increases upon increasing the amounts of PDLA and then reaches an almost constant value when the amount of PDLA in the PLLA phase is up to 20 wt%. For example, the electrical conductivity of the (*x*PLLA + *y*PDLA)/PCL/MWCNT nanocomposites increases from 2.13×10^{-12} S m^{-1} without adding PDLA to 1.07×10^{-5} S m^{-1} with 20 wt% PDLA in the PLLA phase. The increase of electrical conductivity is ascribed to the morphological transformation to form the continuous conductive PCL phase.

Interestingly, the electrical conductivity of the PCL with 0.08 wt% MWCNTs is only 5.0×10^{-12} S m^{-1} (Fig. S3a, ESI†), but it is 1.07×10^{-5} S m^{-1} for the (*x*PLLA + *y*PDLA)/PCL/0.08MWCNT nanocomposites with 20 wt% PDLA in the PLLA phase

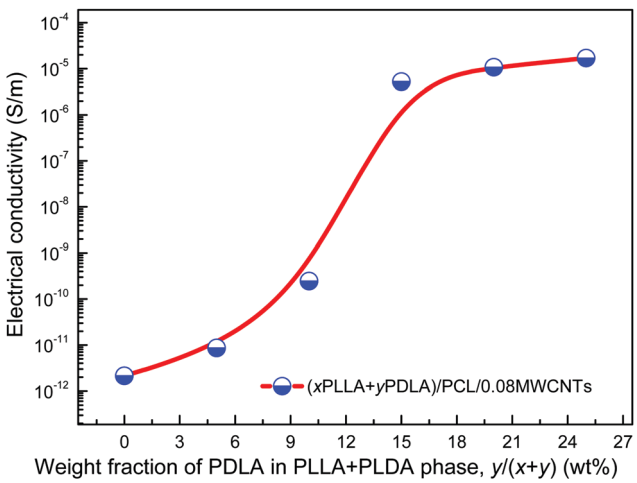

Fig. 5 Effect of PDLA content on the electrical conductivity of the (*x*PLLA + *y*PDLA)/PCL/0.08MWCNTs nanocomposites. The weight ratio of (*x*PLLA + *y*PDLA)/PCL was maintained at 60/40.

(the weight ratio of (*x*PLLA + *y*PDLA)/PCL was maintained to be 60/40). The reasons for the obvious increase in the electrical conductivity are the MWCNTs favorably dispersed in the PCL

phase[47] and the non-conductive PLLA phase acting as the segregated or double percolation structures. Actually, the content of MWCNTs in the PCL phase is about 0.2 wt% for the nanocomposites, where the electrical conductivity of the PCL/MWCNT nanocomposites is 1.4×10^{-5} S m^{-1} (Fig. S3a, ESI†), similar to the value of the (*x*PLLA + *y*PDLA)/PCL/MWCNT nanocomposites with 20 wt% PDLA in the PLLA phase, Fig. 5. The results indicate that 20 wt% of PDLA in the PLLA phase is a prior percentage to organize highly efficient conductive networks in the (*x*PLLA + *y*PDLA)/PCL/MWCNT nanocomposites.

3.3 Conductive networks formed by the morphological transformation

In order to well demonstrate the effects of MWCNTs on the conductive networks in the (*x*PLLA + *y*PDLA)/PCL/MWCNT nanocomposites during the morphological transformation, *x* and *y* are set at 48 and 12 wt% in the whole nanocomposites. Fig. 6a shows the electrical conductivity of the PLLA/PCL/*z*MWCNT nanocomposites without PDLA and the (48PLLA + 12PDLA)/PCL/*z*MWCNT nanocomposites. Expectedly, the addition of PDLA in the PLLA phase can obviously increase the electrical conductivity of the composites. The value of percolation threshold (ϕ_c) was obtained by fitting the variation of electrical conductivity (σ) with MWCNT concentration (ϕ) using eqn (5):[66]

$$\sigma = \sigma_0(\phi - \phi_c)^t \quad (5)$$

where σ_0 is a constant that is typically assigned to the plateau conductivity of fully loaded composites, and t is the scaling exponent which is used to predict the mechanism of network formation. The values of $t \approx 2$ and $t \approx 1.3$ generally reflect three-dimensional and two-dimensional conductive networks, respectively.[67] However, the experimental values usually deviate from these predicted values. Many studies have reported large variations in this exponent from 1 to 12.[68,69] This deviation between the theoretical prediction and the experimental value is still an unresolved issue so far. Nevertheless, it is acceptable that the value of $t > 2$ means three-dimensional conductive networks formed in the composites by the classic percolation theory.[70] In this work, the calculated value of t for the PLLA/PCL/MWCNT nanocomposites increases from 1.64 to 2.66 by adding 20 wt% PDLA in the PLLA phase (Fig. 6b). The results indicate that three-dimensional conductive networks are formed in the PLLA/PCL/MWCNT nanocomposites with 20 wt% PDLA in the PLLA phase to enhance the electrical conductivity.

The percolation threshold (ϕ_c) of the PLLA/PCL/MWCNT nanocomposites is about 0.13 vol%, which is higher than that of the PCL/MWCNT nanocomposites. The ϕ_c of the PCL/MWCNT nanocomposites is 0.086 vol%, also estimated by eqn (3), whereas the critical exponent t is 2.02 (Fig. S3, ESI†). The results indicate that the PLLA/PCL 60/40 matrix without PDLA is harmful to form conductive networks in the PCL phase because the PCL is a dispersion phase in the PLLA/PCL 60/40 blends. However, the ϕ_c of the (48PLLA + 12PDLA)/PCL/MWCNT nanocomposites is reduced to 0.017 vol% because of the morphological transformation to form a co-continuous morphology. There is a 7.7-fold and 5.1-fold decrease in comparison to the PLLA/PCL/MWCNT nanocomposites and the PCL/MWCNT nanocomposites, respectively.

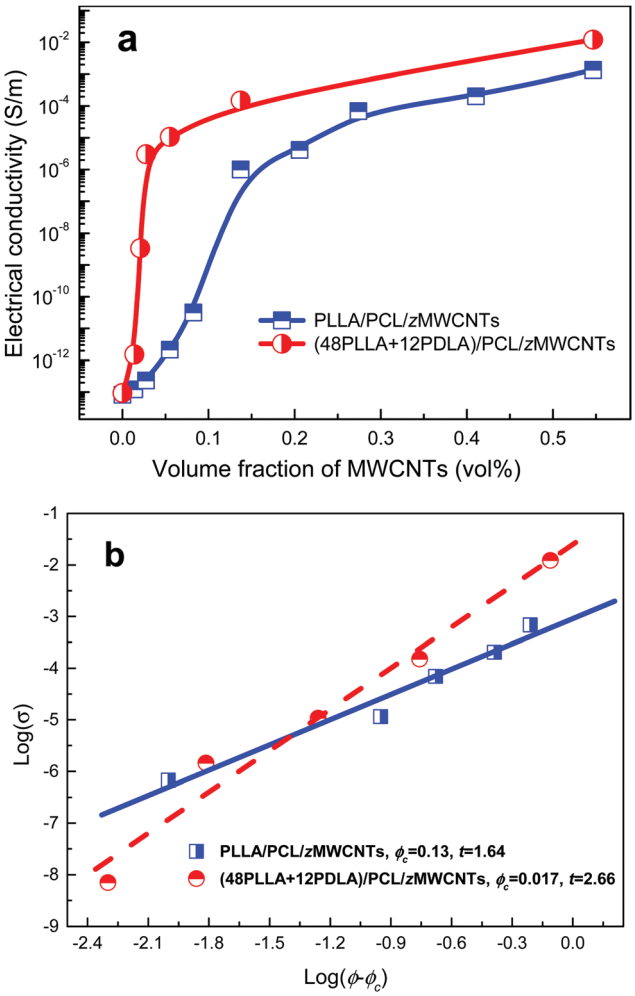

Fig. 6 (a) Electrical conductivity of the PLLA/PCL/*z*MWCNT nanocomposites and the (48PLLA + 12PDLA)/PCL/*z*MWCNT nanocomposites; and (b) the log–log plot of electrical conductivity *versus* $\phi - \phi_c$ for the above nanocomposites.

3.4 EMI shielding behaviors and mechanistic investigation

The high-performance electrical conductivity of the (48PLLA + 12PDLA)/PCL/MWCNT composites was thought to help in developing highly efficient EMI shielding materials, especially at low MWCNT loading. Fig. 7 shows the EMI SE of the (48PLLA + 12PDLA)/PCL/MWCNTs and the PLLA/PCL/MWCNT composites with different MWCNT loadings. The EMI SE also indicates a material's ability to attenuate microwave intensity. For the samples without MWCNTs, the EMI SE is found to be 1.8–6.5 dB, indicating that microwave radiation can easily pass through these samples. The EMI SE of the PLLA/PCL/MWCNT composites exhibits little improvement with increasing MWCNT loading because of the sea-island morphology in the composites. The MWCNTs are confined in the PCL island to have low electrical conductivity, which makes the composites poorly attenuate electromagnetic waves. The EMI SE is only 5.3–8.6 dB for the

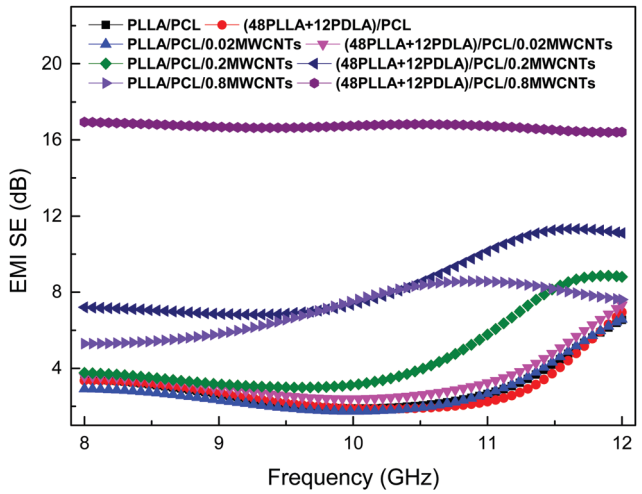

Fig. 7 EMI SE as a function of frequency for the PLLA/PCL/MWCNT and (48PLLA + 12PDLA)/PCL/MWCNT composites with 0, 0.02, 0.2 and 0.8 wt% MWCNT loading, respectively.

PLLA/PCL/0.8MWCNT composites. For the (48PLLA + 12PDLA)/PCL/MWCNT composites with 0.2 and 0.8 wt% MWCNTs, the EMI SE is found to be 7.2–11.4 and ~17 dB, respectively. According to eqn (2), the EMI SE of 17 dB means the blocking of ~98% incident microwave energy in the (48PLLA + 12PDLA)/PCL/MWCNT composites with 0.8 wt% MWCNTs. However, only ~70% incident microwave energy can be blocked by the PLLA/PCL/0.8MWCNT composites. The improved EMI shielding performance is mainly related to the enhanced electrical conductivity of the (48PLLA + 12PDLA)/PCL/MWCNT composites with co-continuous morphology and the increased MWCNT loadings.[71] The results indicate that the EMI SE of the (48PLLA + 12PDLA)/PCL/0.8MWCNT composites is nearly two times higher than that of the PLLA/PCL/0.8MWCNT composites, testifying the great superiority of a co-continuous morphology over a sea-island morphology in improving the EMI SE. Although the EMI SE value of the (48PLLA + 12PDLA)/PCL/0.8MWCNT composites does not reach the level required for common housing electronic

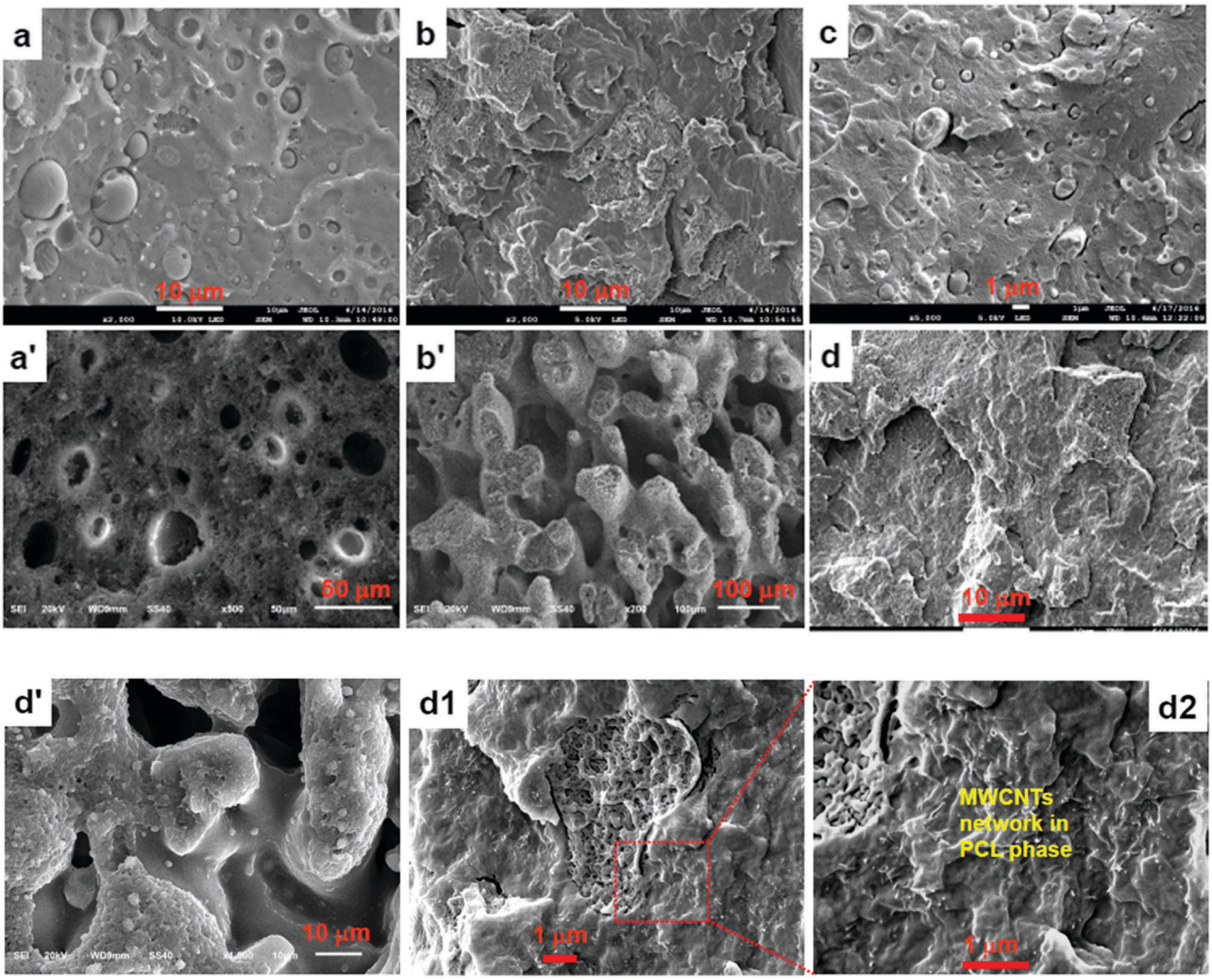

Fig. 8 Effect of MWCNT content on the morphology of the PLLA/PCL/zMWCNT nanocomposites (a and c) and the (48PLLA + 12PDLA)/PCL/zMWCNT nanocomposites (b and d): (a and b) with 0.02 wt% MWCNTs, (c and d) with 0.80 wt% MWCNTs. (d1 and d2) are magnifications of (d) to show the MWCNT network in the PCL phase. The etched surface (the PCL phase is removed) of the composites: (a′) with 0.02 wt% MWCNTs without PDLA, (b′) with 0.02 wt% MWCNTs with 20 wt% PDLA, and (d′) with 0.8 wt% MWCNTs with 20 wt% PDLA.

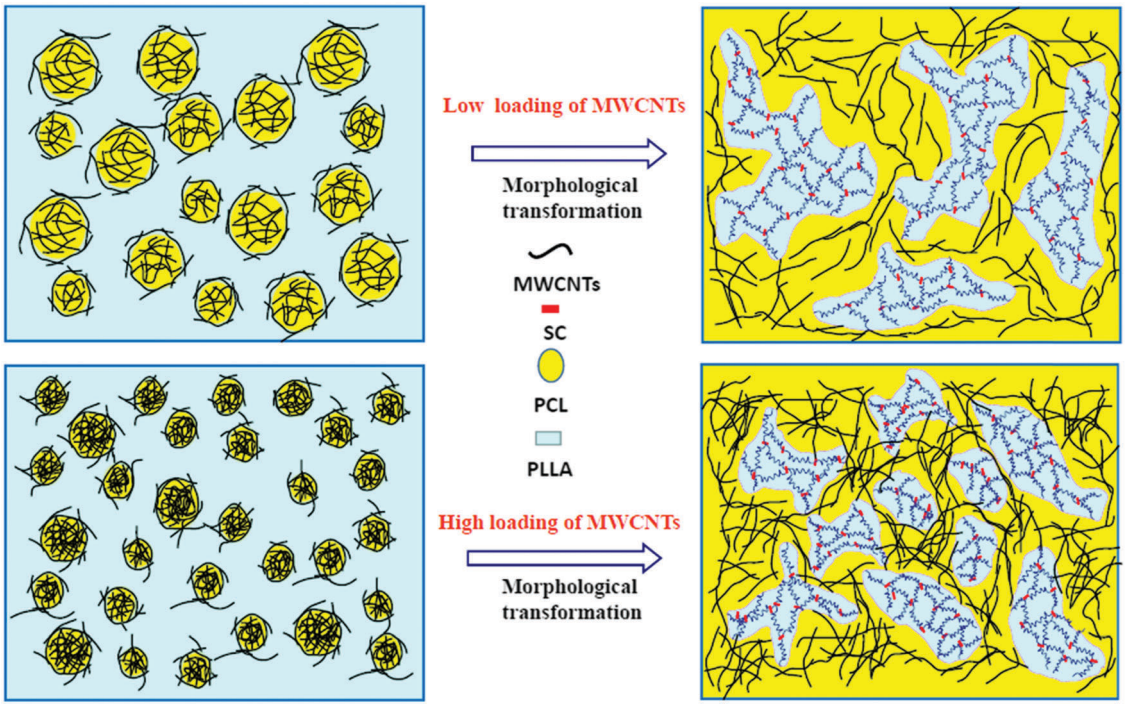

Fig. 9 Schematic illustrations of the morphological transformation and the MWCNT redistribution in PLLA/PCL/MWCNT (PLLA/PCL 60/40) nanocomposites with low and high loadings of MWCNTs with 20 wt% PDLA in the PLLA phase.

equipment (>40 dB), according to the requirements of the Federal Communications Commission,[72] we believe that the EMI SE value of the composites can be further enhanced by adding more MWCNTs through this morphological regulation strategy.

Furthermore, all the samples, except the (48PLLA + 12PDLA)/PCL/0.8MWCNT composites, show frequency dependence across the measured frequency range. The frequency-dependent performance can be attributed to the losses from the dielectric polarizations of MWCNTs in the composites with inferior conductivity.[73] The low electrical conductivity of the composites with sea-island morphology is also thought to be responsible for the frequency-dependent EMI SE performance. For the (48PLLA + 12PDLA)/PCL/0.8MWCNT composites, the EMI SE exhibits weak frequency dependence because of the formation of highly conductive networks therein, and then efficiently improves EMI SE.

Fig. 8 shows the morphological differentiation of the samples without PDLA and with 20 wt% PDLA in the PLLA phase. The morphological transformation, which is from the continuous PLLA phase and the dispersed PCL phase (Fig. 8a and c) to co-continuous morphology (Fig. 8b and d), occurs in all the samples with different contents of MWCNTs. The morphological transformation benefits the formation of conductive networks in the (PLLA + PDLA)/PCL/MWCNT nanocomposites (Fig. 8d1 and d2) and enhances their electrical conductivity.

The effect of MWCNTs on the morphology of the nanocomposites was also discussed together with PDLA. For the samples without PDLA, the incorporation of MWCNTs in the PLLA/PCL/MWCNT nanocomposites reduces the size of the PCL droplets dispersed in the PLLA matrix. The average diameter of the PCL droplets decreases from ~8.0 μm with 0.02 wt% MWCNTs to ~1.0 μm with 0.8 wt% MWCNTs (Fig. 8a and c). The size decrease of the PCL droplets is probably ascribed to the increased viscosity of the PCL phase by adding MWCNTs which also affects the final morphology of the (PLLA + PDLA)/PCL/MWCNT nanocomposites with 20 wt% PDLA in the PLLA phase. The samples with a low loading of MWCNTs lead to a smaller size phase of co-continuous morphology (Fig. 8b′), while the samples with a high loading of MWCNTs result in a larger size phase of co-continuous morphology (Fig. 8d′). Fig. 9 also illustrates the morphological transformation of the nanocomposites with different contents of MWCNTs. The morphological transformation shows high efficiency to organize conductive MWCNT networks in the PCL phase because the MWCNTs are selectively dispersed in the PCL phase and the segregated structures are formed by the dispersed PLLA phase. Different sizes of the phase are probably related to different viscosities of the PCL/MWCNT phase by adding different contents of MWCNTs. High loadings of MWCNTs will lead to higher viscosity of the PCL/MWCNTs phase, which will change the viscosity ratio of the PLLA/PDLA phase, and finally change the size of the co-continuous morphology.

4. Conclusions

Morphological regulation was achieved in PLLA/PCL/MWCNT nanocomposites *via* constructing enough SCs in the PLLA phase. The SCs which were formed during the melt-processing acted as nucleating agents for HCs and rheological modifiers to increase the viscosity and elasticity of the PLLA phase. The increased

viscosity and elasticity made the PLLA shrink and the PCL become a continuous phase from the previously dispersed phase. It was found that the electrical conductivity obviously increased by this morphological transformation because the conductive paths were simultaneously organized when the continuous PCL phase was developed. The electrical conductivity of the PLLA/PCL/MWCNT (PLLA/PCL 60/40) nanocomposites with 0.08 wt% MWCNTs was increased from 2.1×10^{-12} S m^{-1} without adding PDLA to 1.1×10^{-5} S m^{-1} with 20 wt% PDLA in the PLLA phase. The percolation threshold of the PLLA/PCL/MWCNT (PLLA/PCL 60/40) nanocomposites was also reduced from 0.13 vol% to 0.017 vol% by adding 20 wt% PDLA in the PLLA phase. The EMI SE of the (48PLLA + 12PDLA)/PCL/0.8MWCNT composite is nearly twice as high as that of the PLLA/PCL/0.8MWCNT composite because of its unique morphological transformation. Moreover, the electrical conductivity of the nanocomposites could be tuned by changing the amount of PDLA because a different morphology was formed with different amounts of PDLA. This unique morphological transformation can be used to fabricate and design the structure and properties of the PLLA-based polymer blends and composites with potential for EMI shielding applications.

Acknowledgements

The authors are grateful to the National Natural Science Foundation of China (51541306) and the Natural Science Foundation Project of CQ (CSTC2014JCYJA50024) for financial support of this work.

References

1 H. Gu, C. Ma, J. Gu, J. Guo, X. Yan, J. Huang, Q. Zhang and Z. Guo, *J. Mater. Chem. C*, 2016, **4**, 5890–5906.
2 J. Gu, C. Liang, X. Zhao, B. Gan, H. Qiu, Y. Guo, X. Yang, Q. Zhang and D.-Y. Wang, *Compos. Sci. Technol.*, 2017, **139**, 83–89.
3 J. Gu, X. Meng, Y. Tang, Y. Li, Q. Zhuang and J. Kong, *Composites, Part A*, 2017, **92**, 27–32.
4 L. C. Jia, D. X. Yan, C. H. Cui, X. Jiang, X. Ji and Z. M. Li, *J. Mater. Chem. C*, 2015, **3**, 9369–9378.
5 Q. He, T. Yuan, X. Zhang, X. Yan, J. Guo, D. Ding, M. A. Khan, D. P. Young, A. Khasanov, Z. Luo, J. Liu, T. D. Shen, X. Liu, S. Wei and Z. Guo, *J. Phys. Chem. C*, 2014, **118**, 24784–24796.
6 J. Li, H. Liu, J. Guo, Z. Hu, Z. Wang, B. Wang, L. Liu, Y. Huang and Z. Guo, *J. Mater. Chem. C*, 2017, **5**, 1095–1105.
7 H. Liu, J. Gao, W. Huang, K. Dai, G. Zheng, C. Liu, C. Shen, X. Yan, J. Guo and Z. Guo, *Nanoscale*, 2016, **8**, 12977–12989.
8 C. Alippi, *CAAI Transactions on Intelligence Technology*, 2016, **1**, 1–3.
9 H. Liu, Y. Li, K. Dai, G. Zheng, C. Liu, C. Shen, X. Yan, J. Guo and Z. Guo, *J. Mater. Chem. C*, 2016, **4**, 157–166.
10 H. Jin, Q. Chen, Z. Chen, Y. Hu and J. Zhang, *CAAI Transactions on Intelligence Technology*, 2016, **1**, 104–113.
11 H. Liu, W. Huang, X. Yang, K. Dai, G. Zheng, C. Liu, C. Shen, X. Yan, J. Guo and Z. Guo, *J. Mater. Chem. C*, 2016, **4**, 4459–4469.
12 K. Zhang, J.-K. Peng, Y.-D. Shi, Y.-F. Chen, J.-B. Zeng and M. Wang, *J. Phys. Chem. B*, 2016, **120**, 7423–7437.
13 M. Wang, X.-Y. Deng, A.-K. Du, T.-H. Zhao and J.-B. Zeng, *RSC Adv.*, 2015, **5**, 73146–73154.
14 Y.-D. Shi, M. Lei, Y.-F. Chen, K. Zhang, J.-B. Zeng and M. Wang, *J. Phys. Chem. C*, 2017, **121**, 3087–3098.
15 H. Deng, L. Lin, M. Z. Ji, S. M. Zhang, M. B. Yang and Q. Fu, *Prog. Polym. Sci.*, 2014, **39**, 27–655.
16 C. Mao, Y. T. Jiang and W. Jiang, *ACS Appl. Mater. Interfaces*, 2012, **4**, 5281–5286.
17 W. L. Gao, Y. Zheng, J. B. Shen and S. Y. Guo, *ACS Appl. Mater. Interfaces*, 2015, **7**, 1541–1549.
18 K. Zhang, J. K. Peng, Y. D. Shi, Y. F. Chen, J. B. Zeng and M. Wang, *J. Phys. Chem. B*, 2016, **120**, 423–7437.
19 Y. H. Zhan, M. Lavorgna, G. Buonocore and H. S. Xia, *J. Mater. Chem.*, 2012, **22**, 10464–10468.
20 H. Deng, M. Z. Ji, D. X. Yan, S. R. Fu, L. Y. Duan, M. W. Zhang and Q. Fu, *J. Mater. Chem. A*, 2014, **2**, 10048–10058.
21 K. Ke, P. Potschke, N. Wiegand, B. Krause and B. Voit, *ACS Appl. Mater. Interfaces*, 2016, **8**, 14190–14199.
22 G. Nasti, G. Gentile, P. Cerruti, C. Carfagna and V. Ambrogi, *Polymer*, 2016, **99**, 193–203.
23 A. Goeldel, A. Marmur, G. R. Kasaliwal, P. Poetschke and G. Heinrich, *Macromolecules*, 2011, **44**, 6094–6102.
24 E. Cohen, L. Zonder, A. Ophir, S. Kenig, S. McCarthy, C. Barry and J. Mead, *Macromolecules*, 2013, **46**, 1851–1859.
25 X. Huang, Z. Yan, C. M. Huang, H. W. Bai, Q. Zhang and Q. Fu, *Polymer*, 2016, **82**, 11–21.
26 Y. Lan, H. Liu, X. Cao, S. Zhao, K. Dai, X. R. Yan, G. Q. Zheng, C. T. Liu, C. Y. Shen and Z. H. Guo, *Polymer*, 2016, **97**, 11–19.
27 J. Chen, Y. Y. Shi, J. H. Yang, N. Zhang, T. Huang, C. Chen, Y. Wang and Z. W. Zhou, *J. Mater. Chem.*, 2012, **22**, 22398–22404.
28 M. K. Li, C. X. Gao, H. L. Hu and Z. D. Zhao, *Carbon*, 2013, **65**, 371–373.
29 Y.-D. Shi, M. Lei, Y.-F. Chen, K. Zhang, J.-B. Zeng and M. Wang, *J. Phys. Chem. C*, 2017, **121**, 3087–3098.
30 Y. Lin, S. Liu and L. Liu, *J. Mater. Chem. C*, 2016, **4**, 2353–2358.
31 H. Pang, Y. Bao, L. Xu, D. X. Yan, W. Q. Zhang, J. H. Wang and Z. M. Li, *J. Mater. Chem. A*, 2013, **1**, 4177–4181.
32 T. Li, L. F. Ma, R. Y. Bao, G. G. Qi, W. Yang, B. Xie and M. B. Yang, *J. Mater. Chem. A*, 2015, **3**, 5482–5490.
33 J. H. Du, Z. Zhao, Y. Zeng, L. L. Zhang, F. Li, P. F. Liu and C. Liu, *Carbon*, 2011, **49**, 1094–1100.
34 H. Pang, L. Xu, D. X. Yan and Z. M. Li, *Prog. Polym. Sci.*, 2014, **39**, 1908–1933.
35 S. Maiti, S. Suin, N. K. Shrivastava and B. B. Khatua, *RSC Adv.*, 2014, **4**, 7979–7990.
36 K. Hayashida and Y. Matsuoka, *Carbon*, 2015, **85**, 363–371.
37 M. H. Al-Saleh, W. H. Saadeh and U. Sundararaj, *Carbon*, 2013, **60**, 146–156.

38 H. Wang, K. Zheng, X. Zhang, T. Du, C. Xiao, X. Ding, C. Bao, L. Chen and X. Tian, *Composites, Part A*, 2016, **90**, 606–613.
39 C. H. Cui, D. X. Yan, H. Pang, X. Xu, L. C. Jia and Z. M. Li, *ACS Sustainable Chem. Eng.*, 2016, **4**, 4137–4145.
40 L. C. Jia, D. X. Yan, C. H. Cui, X. Ji and Z. M. Li, *Macromol. Mater. Eng.*, 2016, **301**, 1232–1241.
41 D. X. Yan, H. Pang, B. Li, R. Vajtai, L. Xu, P. G. Ren, J. H. Wang and Z. M. Li, *Adv. Funct. Mater.*, 2015, **25**, 559–566.
42 H. W. Bai, H. Xiu, J. Gao, H. Deng, Q. Zhang, M. B. Yang and Q. Fu, *ACS Appl. Mater. Interfaces*, 2012, **4**, 897–905.
43 N. López-Rodríguez, A. López-Arraiza, E. Meaurio and J. R. Sarasua, *Polym. Eng. Sci.*, 2006, **46**, 1299–1308.
44 R. D. Erba, G. Groeninckx, G. Maglio, M. Malinconico and A. Migliozzi, *Polymer*, 2001, **42**, 7831–7840.
45 E. Laredo, M. Grimau, A. Bello, D. F. Wu, Y. S. Zhang and D. P. Lin, *Biomacromolecules*, 2010, **11**, 1339–1347.
46 D. Wu, Y. Zhang, M. Zhang and W. Yu, *Biomacromolecules*, 2009, **10**, 417–424.
47 J. Huang, C. Mao, Y. Zhu, W. Jiang and X. Yang, *Carbon*, 2014, **73**, 267–274.
48 Z. Xu, Y. Zhang, Z. Wang, N. Sun and H. Li, *ACS Appl. Mater. Interfaces*, 2011, **3**, 4858–4864.
49 P. Ma, T. Shen, P. Xu, W. Dong, P. J. Lemstr and M. Chen, *ACS Sustainble Chem. Eng.*, 2015, **3**, 1470–1478.
50 H. Quan, S. J. Zhang, J. L. Qiao and L. Y. Zhang, *Polymer*, 2012, **53**, 4547–4552.
51 D. Y. Bai, H. L. Liu, H. W. Bai, Q. Zhang and Q. Fu, *Sci. Rep.*, 2016, **6**, 20260.
52 Z. Liu, Y. Luo, H. Bai, Q. Zhang and Q. Fu, *ACS Sustainble Chem. Eng.*, 2016, **4**, 1111–1120.
53 H. Yamane, K. Sasai, M. Takano and M. T. M. Takahashi, *J. Rheol.*, 2004, **48**, 599–609.
54 M. S. P. Shaffer and A. H. Windle, *Adv. Mater.*, 1999, **11**, 937–941.
55 B. Krause, T. Villmow, R. Boldt, M. Mende, G. Petzold and P. Pötschke, *Compos. Sci. Technol.*, 2011, **71**, 1145–1153.
56 D. Garlotta, *J. Polym. Environ.*, 2001, **9**, 63–84.
57 G. Loomis, J. Murdoch and K. Gardner, *Polym. Prepr.*, 1990, **31**, 55.
58 Z. Wang, L. Wu, J. Zhou, W. Cai, B. Shen and Z. Jiang, *J. Phys. Chem. C*, 2013, **117**, 5446–5452.
59 Z. Wang, L. Wu, J. Zhou, Z. Jiang and B. Shen, *Nanoscale*, 2014, **6**, 12298–12302.
60 C. Liu, Y. Xu, L. Wu, Z. Jiang, B. Shen and Z. Wang, *J. Mater. Chem. A*, 2015, **3**, 10566–10572.
61 X. L. Zhang, X. M. Zhang, M. T. Yang, S. Yang, H. Wu, S. Y. Guo and Y. Z. Wang, *Compos. Sci. Technol.*, 2016, **136**, 104–110.
62 T. H. Zhao, K. L. Yang, R. T. Zeng, A. K. Du, M. Wang and J. B. Zeng, *Ind. Eng. Chem. Res.*, 2016, **55**, 1881–1889.
63 H. W. Bai, H. L. Liu, D. Y. Bai, Q. Zhang, K. Wang, H. Deng, F. Chen and Q. Fu, *Polym. Chem.*, 2014, **5**, 5985–5993.
64 R. Y. Bao, W. Yang, W. R. Jiang, Z. Y. Liu, B. H. Xie, M. B. Yang and Q. Fu, *Polymer*, 2012, **53**, 5449–5454.
65 D. R. Paul and J. W. Barlow, *J. Macromol. Sci., Polym. Rev.*, 1980, **18**, 109–168.
66 D. Stauffer and A. Aharony, *Introduction to Percolation Theory*, Taylor-Francis, London, UK, 1992.
67 J. P. Clerc, G. Giraud, J. M. Laugier and J. M. Luck, *Adv. Phys.*, 1990, **39**, 191–309.
68 W. Bauhofer and J. Z. Kovacs, *Compos. Sci. Technol.*, 2009, **69**, 1486–1498.
69 S. Vionnet-Menot, C. Grimaldi, T. Maeder, S. Strassler and P. Ryser, *Phys. Rev. B: Condens. Matter Mater. Phys.*, 2005, **71**, 064201.
70 R. Zhang, M. Baxendale and T. Peijs, *Phys. Rev. B: Condens. Matter Mater. Phys.*, 2007, **76**, 195433.
71 M. H. Al-Saleh and U. Sundararaj, *Carbon*, 2009, **47**, 1738–1746.
72 N. F. Colaneri and L. W. Schacklette, *IEEE Trans. Instrum. Meas.*, 1992, **41**, 291–297.
73 K. Hayashida and Y. Matsuoka, *Carbon*, 2015, **85**, 363–371.